Journal of Alloys and Compounds 802 (2019) 6–12

Contents lists available at ScienceDirect

Journal of Alloys and Compounds

journal homepage: http://www.elsevier.com/locate/jalcom

Phase structure dependence of acceptor doping effects in $(Bi_{0.5}Na_{0.5})TiO_3$–$BaTiO_3$ lead-free ceramics

He Qi [a, b], Ruzhong Zuo [b, *], Xuefan Zhou [a], Dou Zhang [a, **]

[a] State Key Laboratory of Powder Metallurgy, Central South University, Changsha, Hunan, 410083, PR China
[b] Institute of Electro Ceramics & Devices, School of Materials Science and Engineering, Hefei University of Technology, Hefei, 230009, PR China

ARTICLE INFO

Article history:
Received 7 April 2019
Received in revised form
3 June 2019
Accepted 8 June 2019
Available online 10 June 2019

Keywords:
Lead-free ceramics
Charged defects
Acceptor doping
Lattice distortion
Ferroelectricity

ABSTRACT

The introduction of acceptor dopants into perovskites is a common method for designing hard piezoelectric ceramics by forming defect dipoles. It is interesting to find that the doping effect of a few amount of MnO_2 in $(Bi_{0.5}Na_{0.5})TiO_3$–$BaTiO_3$ lead-free ceramics significantly depends on the local symmetry. A conventional hardening effect corresponding to an obviously enhanced mechanical quality factor and a decreased piezoelectric coefficient can be generated in the tetragonal phase rich zone, rather than in the rhombohedral-rich zone, where a typically amphoteric characteristic can be observed unexpectedly. The result was well interpreted by means of the formation of a local random field as a result of the local symmetry-breaking effect of point defects after doping MnO_2 in addition to a traditional internal bias field as a result of the pinning effect of defect dipoles. Compared with tetragonal-rich ones, the obviously enhanced random field in rhombohedral-rich compositions tends to induce a weakening ferroelectricity, as evidenced by composition dependent normal ferroelectric-relaxor ferroelectric phase transition. This work provides a new understanding of how charged defects affect the domain stability in the matrix with different symmetries through the competition between random electric fields and internal bias fields.

1. Introduction

Developing high-power piezoelectric materials has been specially required to miniaturize the actuators and transducers, in which the same level of mechanical vibration energy can be obtained in a smaller specimen without temperature rise from internal losses [1,2]. Mechanical losses can be divided into intrinsic and extrinsic parts from the polarization rotation and the domain wall movement under external fields, respectively [3]. Both polarization rotation and domain wall motion can be pinned by internal bias fields (E_i), which can be introduced via acceptor ion doping [4–7]. For the charge balance, acceptor doping will introduce oxygen vacancies, being trapped at the domain walls and forming defect dipoles with the acceptor cations [8–13]. The symmetry of defect dipoles tends to be consistent with the crystal symmetry through the migration of oxygen vacancies, inducing the improved domain configuration stability, the enhanced mechanical quality factor Q_m and the decreased dielectric loss [11,14–17].

Based on a reversible defect-mediated domain switching mechanism, large recoverable electrostrains as well as constricted polarization versus electric field (P-E) loops were obtained in acceptor doped ferroelectric crystals and/or ceramics [8–11,18]. Moreover, by further mediating the state of defect dipoles and domains through poling, aging and fatigue processes, a further enhancement of the electrostrain was realized in hard piezoelectric ceramics, such as acceptor doped $BaTiO_3$ (BT), $(Na_{0.5}K_{0.5})NbO_3$ and $Pb(Zr,Ti)O_3$ (PZT) [14–16]. These results suggest that the hard ceramics may be promising for future novel applications in actuators, ultrasonic motors, transducers and et al. [18].

$(Na_{0.5}Bi_{0.5})TiO_3$ (BNT) based lead free ceramics have been actively studied for replacing lead-based ferroelectric materials [19,20]. Below 255 °C, a rhombohedral (R) R3c structure is stable with anti-phase $a^-a^-a^-$ octahedral tilting and ion displacement along the [111]-direction in the pseudo-cubic cell with α~89.83° [21]. Early reports suggest that the tilted octahedra may strongly affect the domain switching behavior, the dielectric and piezoelectric properties of ceramics and even lead to the formation of pinched or double-like P-E hysteresis loops, which can be explained

* Corresponding author.
** Corresponding author.
E-mail addresses: piezolab@hfut.edu.cn (R. Zuo), dzhang@csu.edu.cn (D. Zhang).

https://doi.org/10.1016/j.jallcom.2019.06.102
0925-8388/

in terms of domain wall pinning through oxygen octahedra rotations in unpoled R3c PZT ceramics [22]. BNT ceramics exhibit a stable domain configuration, a large coercive field (E_C) ~7.3 kV/mm and a large Q_m~400 [23]. However, a pinched P-E loop has not been found, as usually observed in conventional PZT ceramics. Acceptor doping has been tried in BNT-based ceramics in order to further inhibit the motion of polarization and domain walls, however, the enhancement of Q_m value is very little [7,24–27]. Moreover, typical constricted P-E loops were also not found. Instead, softening characteristics such as increased d_{33}, decreased depolarization temperature and decreased E_C were observed in BNT ceramics after doping a small content of MnO_2 [28].

In this work, a special study on the effect of acceptor doping MnO_2 in BNT-based ceramics with different local structures has been carried out to reveal the structure mechanism for producing BNT-based hard piezoelectric ceramics.

2. Experimental procedures

Ceramics with compositions of (1-x)BNT-xBT-yMnO_2 (x = 0–0.4, y = 0–0.01) were synthesized by a conventional solid-state reaction method. Commercially available reagent grade oxide and carbonate powders Na_2CO_3 (≥99.8%), $BaCO_3$ (≥99.5%), Bi_2O_3 (≥99.5%), TiO_2 (≥99.5%) and MnO_2 (≥99.5%) (Sinopharm Chemical Reagent Co., Ltd., CN) were used as the starting materials. The powders for (1-x)BNT-xBT were weighed and mixed thoroughly in ethanol using zirconia balls for 6 h according to their compositional formula. The mixed powder was then calcined at 850 °C for 2 h. MnO_2 was added according to its doping content. The powders were ball-milled again for 12 h and then pressed into disk samples with a diameter of 10 mm under 100 MPa using polyvinyl alcohol as the binder. After burning out the binder at 550 °C for 4 h, sintering was performed in the temperature range of 1140–1180 °C for 2 h at a heating rate of 180 °C/h and a cooling rate of 300 °C/h in covered alumina crucibles. Silver electrodes were fired on both sides of the samples at 550 °C for 30 min. The samples were poled at 70–120 °C in a silicone oil bath with a dc electric field of 7 kV/mm for 2 h. After poling, the samples were aged for at least 24 h before electrical performance testing.

The domain morphology observation was performed on a field emission transmission electron microscope (FE-TEM, JEM-2100F, JEOL, Japan) operated at 200 kV. X-ray photoelectron spectroscopy (XPS, Escalab 250Xi; Thermo Scientific, Leicestershire, U.K.) was utilized to determine the valence of manganese in the compounds. Dielectric properties as a function of temperature and frequency were measured by an LCR meter (Agilent E4980A, Santa Clara, CA). The quasi-static piezoelectric constant d_{33} was measured by a Berlincourt-meter (YE2730A, Sinocera, Yangzhou, China) and the Q_m was determined by a resonance-antiresonance method with an impedance analyzer (PV70A, Beijing Band ERA Co., Ltd. China). The P-E loops were measured at 10 Hz using a ferroelectric test system (Precision multiferroelectric; Radiant Technologies Inc, Albuquerque, New Mexico). The room temperature crystal structure was analyzed by a powder X-ray diffractometer (XRD, D/MAX-RB, Rigaku, Tokyo, Japan) using a Cu Kα radiation (λ = 1.5406 Å).

3. Results and discussion

The domain morphology for several selected (1-x)BNT-xBT ceramics is shown in Fig. 1. For pure BNT ceramic (x = 0) with an R symmetry, an irregular domain morphology with size around 50–100 nm can be observed in Fig. 1a. The coexistence of nano-domains with blotchy domain morphology and stripe micro-domains can be observed on a bright-field image of the morphotropic phase boundary (MPB) composition with x = 0.06. Typical 90° domains with parallel strips can be observed in the tetragonal (T) phase composition with x = 0.12, which can be described as the alternation of broad and narrow sub-micron sized domains.

Fig. 2 presents high-resolution XPS spectra of Mn 2p states for as-sintered (1-x)BNT-xBT-0.01MnO_2 ceramics. The overlapped Mn $2p_{3/2}$ and $2p_{1/2}$ peaks were fitted to analyze the different valence states of the doped Mn ions, because Mn has multiple accessible valence states. As exemplified in the Mn $2p_{3/2}$ state, the existence of Mn^{2+} and Mn^{3+} is evident because the peaks are located at the binding energies of ~640.7 and ~641.6 eV, respectively. Therefore, Mn^{2+} and Mn^{3+} ions can coexist in all (1-x)BNT-xBT-0.01MnO_2 ceramics. Moreover, the ratio between Mn^{2+} and Mn^{3+} ions changes little with changing BT content. Generally, Mn^{2+} and Mn^{3+} ions tend to substitute B-site ions in the perovskite structure because the radius of Mn^{2+} (0.83 Å) and Mn^{3+} (0.645 Å) is close to that of Ti^{4+} (0.605 Å). Therefore, charged defects of Mn''_{Ti}, Mn'_{Ti} and $V_O^{\cdot\cdot}$ should be formed in the studied (1-x)BNT-xBT-0.01MnO_2 compositions.

Fig. 3 shows temperature and frequency dependent dielectric permittivity and loss tangent for unpoled and poled (1-x)BNT-xBT-yMnO_2 ceramics. For the composition of y = 0, an obvious dielectric anomaly due to the ferroelectric-relaxor phase transition (T_{FR}) can

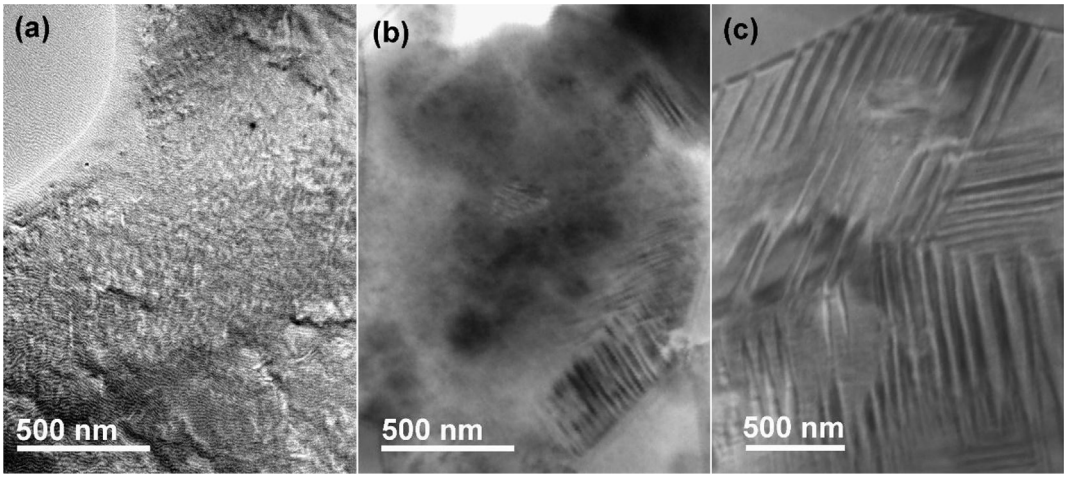

Fig. 1. Bright-field TEM images for (1-x)BNT-xBT ceramics with (a) x = 0, (b) x = 0.06 and (c) x = 0.12.

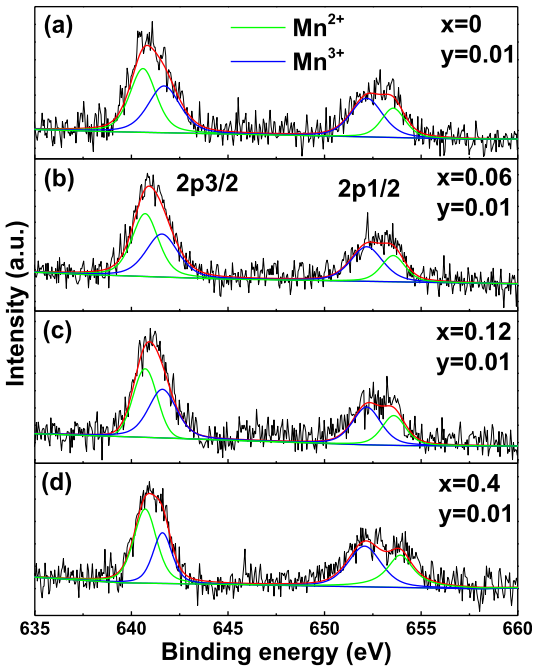

Fig. 2. XPS spectra of Mn 2p for (1-x)BNT-xBT-0.01MnO_2 ceramics with (a) x = 0, (b) x = 0.06, (c) x = 0.12 and (d) x = 0.4.

be seen on heating in the x<0.06 and x>0.09 compositions, corresponding to normal ferroelectric states with R and T phase structures at room temperature, respectively. Even though T_{FR} disappears in the MPB compositions of $0.06 \leq x \leq 0.09$, a significant dielectric anomaly and a sharp loss tangent peak can be detected after poling at room temperature. This indicates that the virgin samples of $0.06 \leq x \leq 0.09$ should be a nonergodic relaxor state at room temperature, and that the field induced ferroelectric phase should transform into ergodic relaxor phase transition at T'_{FR} on heating. T'_{FR} can also be detected in compositions away from the MPB.

After doping 1 mol% MnO_2, all samples exhibit weaker frequency dispersion in the low temperature region by comparing with the corresponding undoped ones. This indicates that the introduction of MnO_2 tends to decrease the dielectric relaxation behavior. However, for the virgin samples of x = 0.045 and x = 0.12, which are close to the MPB and exhibit normal ferroelectric states at room temperature before MnO_2 doping, a nonergodic relaxor state is detected after MnO_2 doping. This suggests an obvious decrease of the domain size from microdomains to polar nanoregions (PNRs) at room temperature, accompanying the decrease of ferroelectricity.

The ferroelectricity at room temperature can be easily evaluated by the Curie temperature, namely the frozen temperature (T_f) or T_{FR} in relaxor ferroelectrics. In consideration of the difficulty in calculating T_f of the virgin sample, a similar temperature T'_{FR} in the poled sample was used [29]. The evolution of T'_{FR} for the (1-x)BNT-xBT-yMnO_2 is shown in Fig. 4a. With increasing BT content, the T'_{FR}

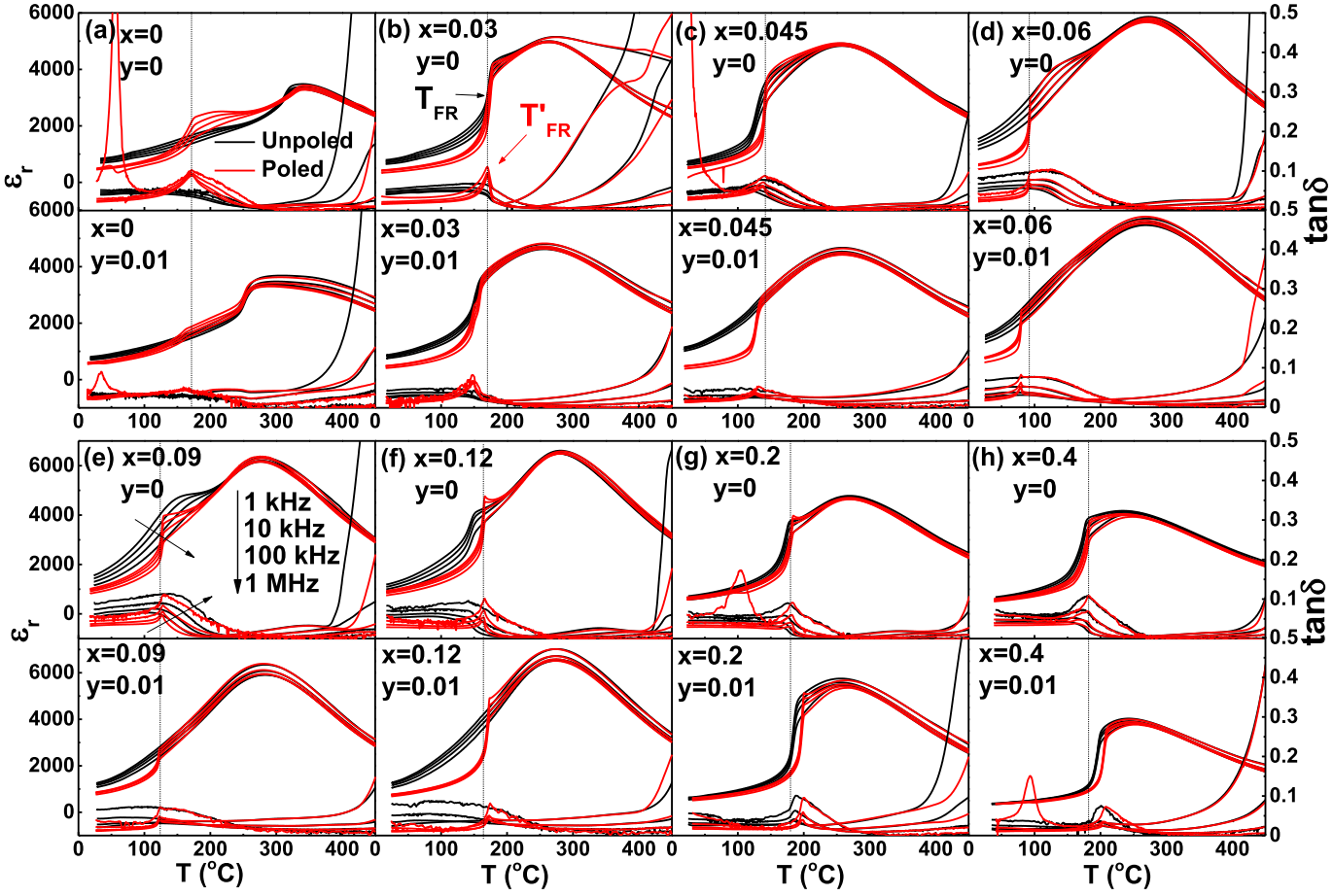

Fig. 3. Temperature and frequency dependent dielectric permittivity and loss tangent for unpoled and poled (1-x)BNT-xBT-yMnO_2 ceramics.

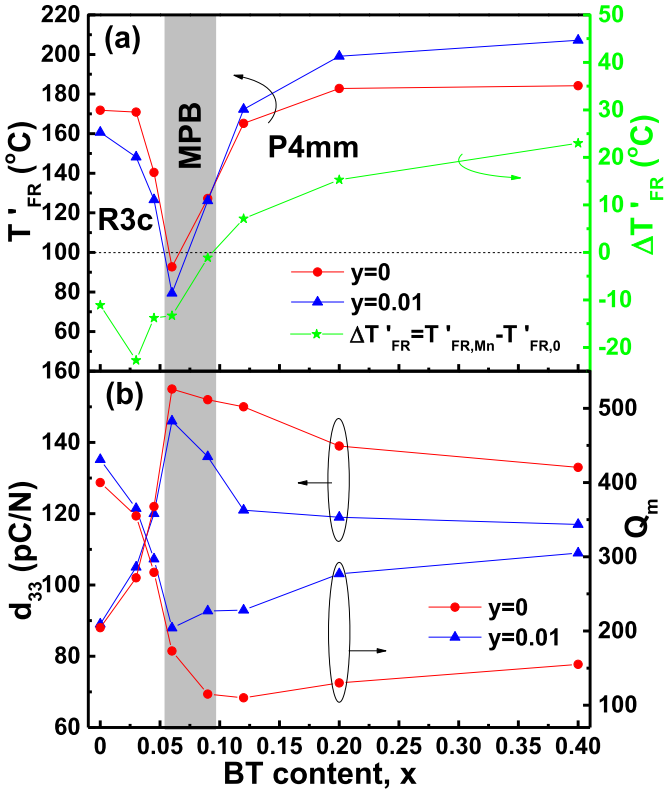

Fig. 4. Evolution of (a) T'_{FR} and $\Delta T'_{FR}$, (b) d_{33} and Q_m with changing BT content for poled (1-x)BNT-xBT-yMnO_2 ceramics.

values for both y = 0 and y = 0.01 ceramics first decrease and then reach minimum values at x = 0.06 and finally increase. Interestingly, after the addition of MnO_2, T'_{FR} decreases slightly for the R-phase rich compositions with x < 0.09, but increases for the T-phase rich compositions with x > 0.09, as compared with the corresponding undoped ones. The difference of T'_{FR} between y = 0.01 and y = 0 ($\Delta T'_{FR} = T'_{FR,Mn}$-$T'_{FR,0}$) tends to increase monotonously from negative to positive values with increasing x. $\Delta T'_{FR}$ approximates to zero in the MPB composition with x = 0.09. These results suggest that the BNT-BT materials with R and T phases should be softened and hardened by acceptor-type dopants, respectively. d_{33} decreases and Q_m increases significantly in the T phase composition after doping MnO_2, as shown in Fig. 4b. By comparison, the influence of MnO_2 on d_{33} and Q_m is much weaker in the R phase composition. As a result, MnO_2 exhibits an amphoteric doping effect in the R phase but a typical hard doping effect in the T phase.

Fig. 5a and b shows the P-E loops and the corresponding J-E curves for unpoled and poled (1-x)BNT-xBT-0.01MnO_2 ceramics. Square and symmetric P-E loops as well as unimodal J-E curves were achieved in the unpoled (1-x)BNT-xBT-0.01MnO_2 ceramics. For typical hard ceramics, pinched and even double P-E loops cab be detected in the unpoled ceramics because the domains in the randomly oriented state are pinned by defect dipoles [11]. However, The E_i formed by the defect dipoles is not large enough to turn back the reoriented domains to the initial random state or even the defect dipoles are not formed in these acceptor doped BNT-BT ceramics. The defect dipoles are formed through the migration of oxygen vacancies, yet large coercive field which hinders the displacement of ions would also block the migration of oxygen vacancies, moreover, driving force originating from the inconsistence between spontaneous polarization (P_S) and defect polarization (P_D) is quite small owing to the existence of nanosized domains. As a result, weak E_i can be detected in these virgin samples. After adequate poling, long-range ordered domains paralleled to the direction of external electric field will be achieved. Moreover, external electric fields tend to accelerate the migration of oxygen vacancies and the formation of defect dipoles along the direction of electric field, leading to the formation of E_i along the direction of electric field. The E_i value can be calculated through the unequal value of E_C during loading positive and negative fields as $E_i=(E_{+}+E_{-})/2$. The poled samples with low BT contents exhibit a nearly symmetric P-E loop. However, an obvious asymmetric P-E loop and an asymmetric J-E curve are found in the poled compositions with high BT contents, as shown in Fig. 5b. The evolution of E_C (for unpoled samples) and E_i (for poled samples) with changing BT content for (1-x)BNT-xBT-0.01MnO_2 ceramics is shown in Fig. 5c. Even though pure BNT exhibits nanoscale domains at room temperature, a large E_C ~7.1 kV/mm can be detected owing to the inhibition of octahedral tilting on domain switching behavior. Accompanying with the decreased domain size, E_C decreases when the composition moves close to the MPB. A minimum E_C can be found in the MPB region. A very small E_i of <0.2 kV/mm can be detected in the R rich compositions with $x \leq 0.06$. With increasing the BT content into the T phase rich zone, E_i increases monotonously. That is to say, the domains in the R phase can hardly be clamped by defect dipoles. Even for the T compositions with large E_i, the value of E_i is still much smaller than that of E_C. A large E_i~1.4 kV/mm and a large E_C~4.5 kV/mm are achieved in the ceramic with x = 0.4. Therefore, the domains cannot switch spontaneously after removing the external field.

The phase structural change in (1-x)BNT-xBT-yMnO_2 ceramics with different x and y values is shown in Fig. 6a and b. It is obvious that all studied compositions demonstrate a single perovskite structure in terms of typical diffraction patterns. Fig. 6c–e shows the enlarged (111) and (200) diffraction lines as well as the fitting results to analyze the effect of BT and MnO_2 on the phase structure and ferroelectricity. The doublet $(111)_R/(11\text{-}1)_R$ and single $(200)_R$ diffraction peaks suggest an R symmetry for the BNT ceramic (x = 0, y = 0). The splitting of $(111)_R$ and $(11\text{-}1)_R$ lines tends to merge together while the (200) diffraction tends to split with increasing BT content. A single (111) peak as well as a doublet (200) peak appears for the x > 0.09 compositions with a pure T symmetry. In the composition range of $0.06 \leq x \leq 0.09$, doublet (111) peaks and triplet (200) peaks can be observed, indicating the coexistence of R and T phases. After the addition of MnO_2, an MPB can still be detected in the composition range of $0.06 \leq x \leq 0.09$, as shown in Fig. 6c–e. An obvious shift of the diffraction peaks owing to the change of the lattice parameters can be found after doping MnO_2, indicating that $Mn^{2+/3+}$ ions have diffused into the crystal lattice.

The lattice parameters of both T and R phases can be calculated according to the position of (111) and (200) diffraction peaks. For the T structure, the interplanar spacings (d), which can be obtained from XRD data by using the Bragg equation, is given as:

$$d_{hkl} = \frac{1}{\sqrt{\left(\frac{h^2+k^2}{a^2} + \frac{l^2}{c^2}\right)}} \quad (1)$$

Therefore, approximate values of c_T and a_T can be obtained by the measurement of (200) line:

$$c_T = 2d_{002} \quad (2)$$

$$a_T = 2d_{200} \quad (3)$$

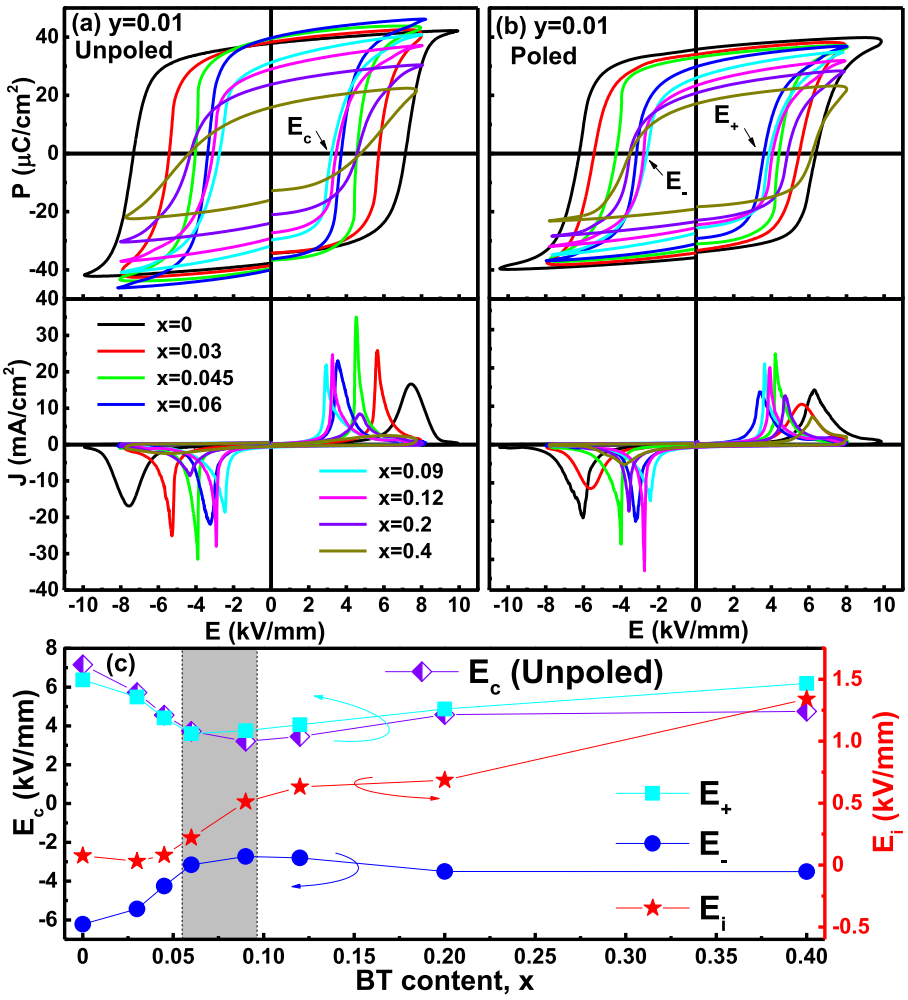

Fig. 5. P–E loops and the corresponding J-E curves for (a) unpoled and (b) poled (1-x)BNT-xBT-0.01MnO_2 ceramics; (c) evolution of E_C and E_i values with changing BT content for unpoled and poled (1-x)BNT-xBT-0.01MnO_2 ceramics.

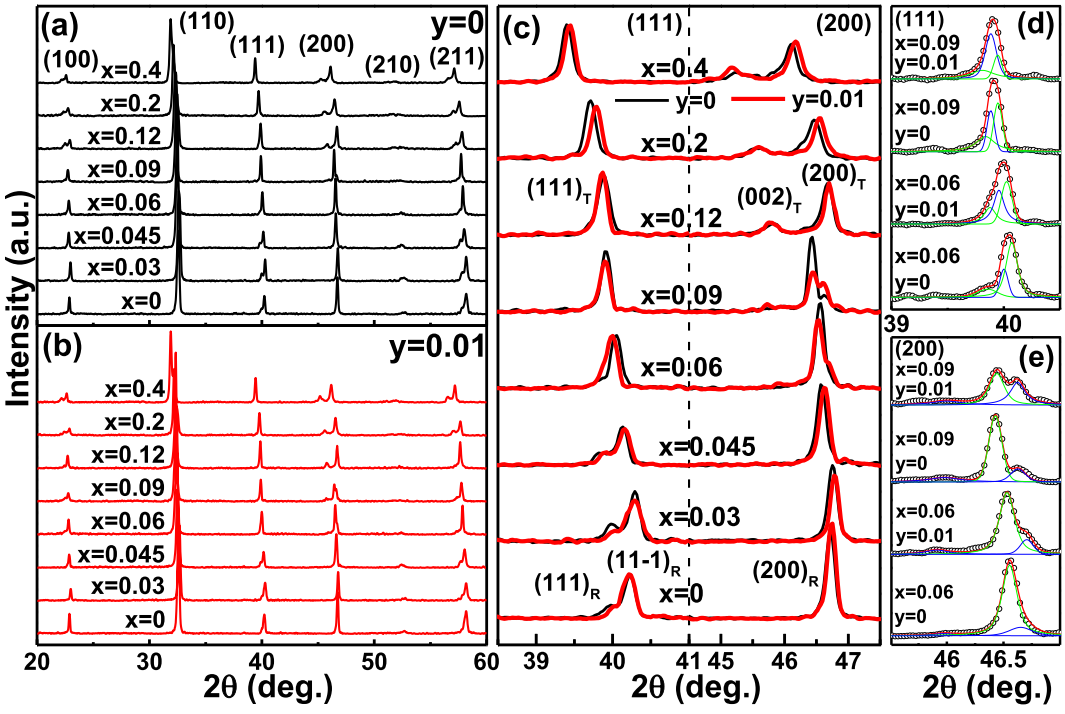

Fig. 6. XRD patterns of (a) y = 0 and (b) y = 0.01 ceramics; (c) evolution of (111) and (200) diffraction lines and (d)(e) the fitting results for (1-x)BNT-xBT-yMnO_2 ceramics.

For the R phase with an internal angle α between the R axes, the interplanar spacings can be written as (without consideration of terms in $\cos^2\alpha$ and $\cos^3\alpha$):

$$d_{hkl} = \left(\frac{h^2+k^2+l^2}{a^2} - 2\frac{hk+kl+lh}{a^2}\cos\alpha\right)^{-\frac{1}{2}} = \frac{a}{\sqrt{h^2+k^2+l^2}}\left(1+\frac{hk+kl+lh}{\sqrt{h^2+k^2+l^2}}\cos\alpha\right) \quad (4)$$

Accordingly, the a_R and α values in R phase can be achieved by:

$$a_R = 2d_{200} \quad (5)$$

$$\cos\alpha = \frac{3(d_{111} - d_{11\bar{1}})}{4a_R} \quad (6)$$

The evolution of lattice parameters and phase fraction is displayed in Fig. 7a. An MPB can be achieved in the composition range of $0.06 \le x \le 0.09$ for both $y = 0$ and $y = 0.01$ ceramics, even though a slight decline of volume fraction of R phase can be observed after doing MnO_2. The lattice distortion of R (90-α) and T (c_T/a_T) phases is displayed in Fig. 7b. It can be found that the lattice distortion of both R and T phases decreases as the MPB is approached for both $y = 0$ and $y = 0.01$ compositions. Interestingly, with the addition of MnO_2, the value of 90-α decreases while c_T/a_T increases as compared with the corresponding undoped ones. Lattice distortion is a key factor affecting the piezoelectric coefficient and dielectric properties (T_{FR} and T'_{FR}) in BNT-based ceramics [30]. As the distortion of lattice becomes smaller, relatively small strains between domains would be induced during poling process, causing easier domain switching and better domain alignment. As a result, a higher piezoelectric response can be achieved. The smaller lattice distortion relative to the cubic phase also means that domains can become more easily randomized on heating, resulting in lower T'_{FR}. The obviously decreased lattice distortion in R phase compositions leads to the decrease of T'_{FR}, indicating that the addition of MnO_2 can increase the activity of the domains. However, the slightly increased Q_m after doing MnO_2 suggests the actual existence of pinning effect, which originates from defect dipoles and tends to decrease the activity of the domains. The introduction of point defects would cause the change of lattice distortion, resulting in a local symmetry-breaking of the Landau free energy curves, as shown in Fig. 7c [31]. Moreover, this local symmetry-breaking effect from point defects exists at all temperatures. The existence of point defect tends to clamp the formation of arranged polarization around it, behaving like a random field. The formation of random field by the point defect tends to break the long range ordered ferroelectric domains, causing the decrease of lattice distortion and domain size, e.g. the formation of nonergodic relaxor phases in $x = 0.045$ and $x = 0.12$ ceramics (Fig. 3). Differently, the internal bias field appears after the formation of defect dipoles through the migration of oxygen vacancies, leading to the decreased dielectric dispersion, reduced piezoelectric response and increased Q_m. Owing to their competitions in the acceptor doped ceramics, different behavior can be observed when the local structure is different. Internal bias field plays a dominant role in the T phase. A more stable domain structure owing to both increased lattice distortion and pinning effect can be achieved in T rich compositions after doping acceptor dopants, causing an obvious hardening behavior. The effect of random field becomes more and more significant as the composition enters the R phase zone, resulting in an amphoteric behavior in the composition with an R symmetry. The appearance of this unusual phenomenon might be related to the relationship between P_S and P_D. Defect symmetry tends to follow

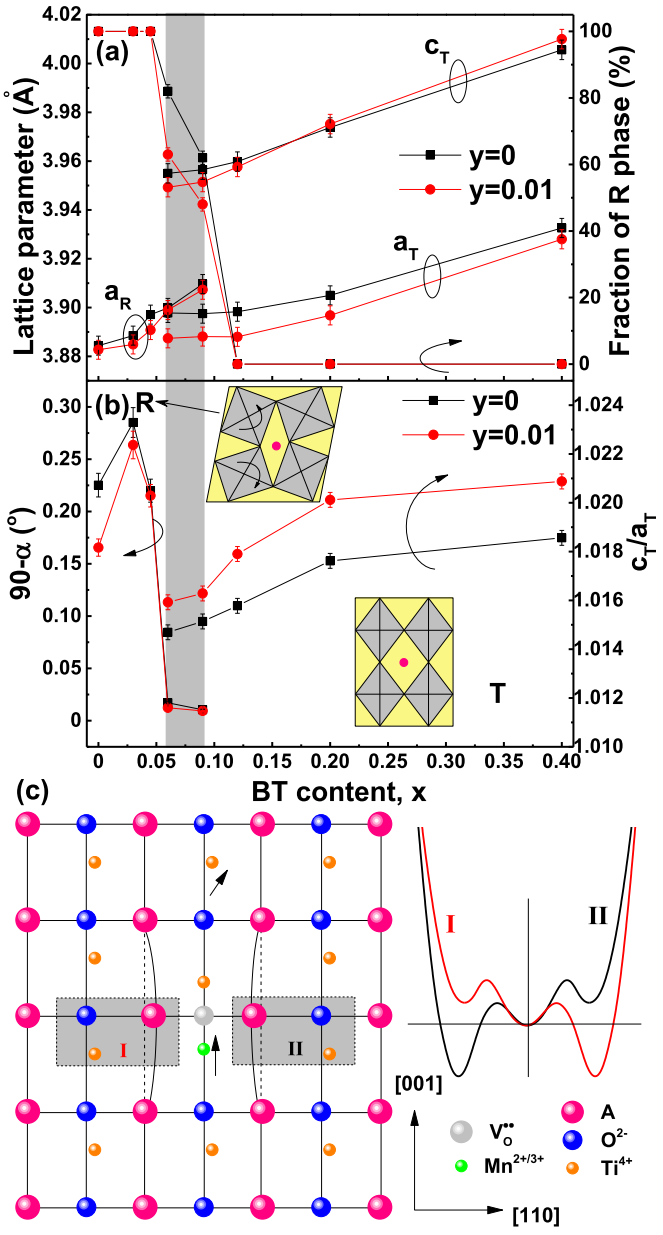

Fig. 7. Evolution of (a) lattice parameters and the fraction of R phase and (b) lattice distortion degree for (1-x)BNT-xBT-yMnO_2 ceramics; (c) the schematic picture of atoms, local symmetry, and local Landau potential around defects in the matrix of R phase.

crystal symmetry in T phase domains as its polarization mainly originates from ions asymmetric displacement, causing the pinning of domains. However, the octahedral tilting plays important roles to the P_S in R phase, thus P_D is hard to conform to P_S.

4. Conclusions

In summary, a fixed content of acceptor dopant MnO_2 was introduced into BNT-BT lead-free ceramics, leading to completely diverse effects in compositions with different phase structures as a result of the competition between the internal bias fields through defect dipoles and the random field owing to the existence of point defects. As a result, a decreased T'_{FR}, a decreased lattice distortion as

well as a nearly symmetric square *P-E* loop can be found in the R phase rich compositions after the addition of MnO_2, indicating an obviously decreased ferroelectricity as well as a typical amphoteric characteristic owing to an enhancing random field in R-rich compositions. By comparison, MnO_2 doped T phase-rich compositions have much smaller random fields than internal bias fields, thus behaving like an obvious hardening feature. The variation of the random field and internal bias field can be manifested by the change of dielectric permittivity versus temperature curves and P-E loops for unpoled and poled samples.

Acknowledgements

This work was financially supported by the China Postdoctoral Science Foundation (Grant No. 2018M642998), Natural Science Foundation of Hunan Provincial (2019JJ50834), Postdoctoral Science Foundation of Central South University (Grant No. 140050027) and Open Sharing Fund for the Large-scale Instruments and Equipment of Central South University.

References

[1] K. Uchino, Piezoelectric ultrasonic motors: overview, Smart Mater. Struct. 7 (1998) 273–285.
[2] T.R. Gururaja, W. Schulze, L.E. Cross, R.E. Newnham, Piezoelectric composite materials for ultrasonic transducer applications. Part II: evaluation of ultrasonic medical applications, IEEE Trans. Son. Ultrason. 32 (1985) 499–513.
[3] L.M. Zheng, L.Y. Yang, Y.R. Li, X.Y. Lu, D. Huo, W.M. Lü, R. Zhang, B. Yang, W.W. Cao, Origin of improvement in mechanical quality factor in acceptor-doped relaxor-based ferroelectric single crystals, Phys. Rev. Appl. 9 (2018) 064028.
[4] D.M. Lin, K.W. Kwok, H.L.W. Chan, Double hysteresis loop in Cu-doped $K_{0.5}Na_{0.5}NbO_3$ lead-free piezoelectric ceramics, Appl. Phys. Lett. 90 (2007) 232903.
[5] X.B. Ren, K. Otsuka, Universal symmetry property of point defects in crystals, Phys. Rev. Lett. 85 (2000) 1016.
[6] H.J. Lee, S.O. Ural, L. Chen, K. Uchino, S.J. Zhang, High power characteristics of lead-free piezoelectric ceramics, J. Am. Ceram. Soc. 95 (2012) 3383–3386.
[7] E. Taghaddos, M. Hejazi, A. Safari, Electromechanical properties of acceptor-doped lead-free piezoelectric ceramics, J. Am. Ceram. Soc. 97 (2014) 1756–1762.
[8] J. Fu, R.Z. Zuo, H. Qi, C. Zhang, J.F. Li, L.T. Li, Low electric-field driven ultrahigh electrostrains in Sb-substituted (Na,K)NbO_3 lead-free ferroelectric ceramics, Appl. Phys. Lett. 105 (2014) 242903.
[9] J.H. Kim, D.H. Kim, T.H. Lee, T.G. Lee, J.H. Lee, B.Y. Kim, S. Nahm, C.Y. Kang, J. Ryu, Large electrostrain in $K(Nb_{1-x}Mn_x)O_3$ lead-free piezoelectric ceramics, J. Am. Ceram. Soc. 99 (2016) 4031–4038.
[10] W.W. Gao, J. Lv, X.J. Lou, Large electric-field-induced strain and enhanced piezoelectric constant in CuO-modified $BiFeO_3$-$BaTiO_3$ ceramics, J. Am. Ceram. Soc. 101 (2018) 3383–3392.
[11] X.B. Ren, Large electric-field-induced strain in ferroelectric crystals by point-defect-mediated reversible domain switching, Nat. Mater. 3 (2004) 91–94.
[12] D. Lee, B.C. Jeon, S.H. Baek, S.M. Yang, Y.J. Shin, T.H. Kim, Y.S. Kim, J.G. Yoon, C.B. Eom, T.W. Noh, Active control of ferroelectric switching using defect-dipole engineering, Adv. Mater. 24 (2012) 6490–6495.
[13] C.B. Long, H.Q. Fan, M.M. Li, A ferroelectric polarization contribution from defect dipoles in acceptor Aurivillius oxide, $(Na,Bi)_{0.47}(Li,Ce)_{0.03}Bi_2Ta_{1.97}Sc_{0.03}O_{8.97}$, Appl. Phys. Lett. 103 (2013) 192908.
[14] X.B. Zhao, R.H. Liang, W.B. Zhang, G.S. Wang, X.L. Dong, Large electrostrain in poled and aged acceptor-doped ferroelectric ceramics via reversible domain switching, Appl. Phys. Lett. 105 (2014) 262902.
[15] J.G. Hao, Z.J. Xu, R.Q. Chu, W. Li, J. Du, P. Fu, G.R. Li, Electric field cycling induced large electrostrain in aged $(K_{0.5}Na_{0.5})NbO_3$–Cu lead-free piezoelectric ceramics, J. Am. Ceram. Soc. 99 (2016) 402–405.
[16] Z. Feng, X.B. Ren, Aging effect and large recoverable electrostrain in Mn-doped $KNbO_3$-based ferroelectrics, Appl. Phys. Lett. 91 (2007), 032904.
[17] P. Marton, C. Elsässer, Switching of a substitutional-iron/oxygen-vacancy defect complex in ferroelectric $PbTiO_3$ from first principles, Phys. Rev. B 83 (2011), 020106.
[18] J.G. Hao, W. Li, J.W. Zhai, H. Chen, Progress in high-strain perovskite piezoelectric ceramics, Mater. Sci. Eng. R 135 (2019) 1–57.
[19] D. Schütz, M. Deluca, W. Krauss, A. Feteira, T. Jackson, K. Reichmann, Lone-pair-induced covalency as the cause of temperature- and field-induced instabilities in bismuth sodium titanate, Adv. Funct. Mater. 22 (2012) 2285–2294.
[20] W. Jo, R. Dittmer, M. Acosta, J.D. Zang, C. Groh, E. Sapper, K. Wang, J. Rödel, Giant electric-field-induced strains in lead-free ceramics for actuator applications–status and perspective, J. Electroceram. 29 (2012) 71–93.
[21] G.O. Jones, P.A. Thomas, Investigation of the structure and phase transitions in the novel A-site substituted distorted perovskite compound $Na_{0.5}Bi_{0.5}TiO_3$, Acta Crystallogr. B. 58 (2002) 168–178.
[22] T. Rojac, S. Drnovsek, A. Bencan, B. Malic, D. Damjanovic, Role of charged defects on the electrical and electromechanical properties of rhombohedral $Pb(Zr,Ti)O_3$ with oxygen octahedra tilts, Phys. Rev. B 93 (2016), 014102.
[23] T. Takenaka, K.I. Maruyama, K. Sakata, $(Bi_{1/2}Na_{1/2})TiO_3$-$BaTiO_3$ system for lead-free piezoelectric ceramics, Jpn. J. Appl. Phys. 30 (1991) 2236–2239.
[24] E. Aksel, P. Jakes, E. Erdem, D.M. Smyth, A. Ozarowski, J.V. Tol, J.L. Jones, R.A. Eichel, Processing of manganese-doped $[Bi_{0.5}Na_{0.5}]TiO_3$ ferroelectrics: reduction and oxidation reactions during calcination and sintering, J. Am. Ceram. Soc. 94 (2011) 1363–1367.
[25] H.C. Hu, M.K. Zhu, F.Y. Xie, N. Lei, J. Chen, Y.D. Hou, H. Yan, Effect of Co_2O_3 additive on structure and electrical properties of $85(Bi_{1/2}Na_{1/2})TiO_3$–$12(Bi_{1/2}K_{1/2})TiO_3$–$3BaTiO_3$ lead-free piezoceramics, J. Am. Ceram. Soc. 92 (2009) 2039–2045.
[26] E. Aksel, E. Erdem, P. Jakes, J.L. Jones, R.A. Eichel, Defect structure and materials "hardening" in Fe_2O_3-doped $[Bi_{0.5}Na_{0.5}]TiO_3$ ferroelectrics, Appl. Phys. Lett. 97 (2010), 012903.
[27] R. Beanland, P.A. Thomas, Symmetry and defects in rhombohedral single-crystalline $Na_{0.5}Bi_{0.5}TiO_3$, Phys. Rev. B 89 (2014) 174102.
[28] Y.C. Guo, H.Q. Fan, C.B. Long, J. Shi, L. Yang, S.H. Lei, Electromechanical and electrical properties of $Bi_{0.5}Na_{0.5}Ti_{1-x}Mn_xO_{3-\delta}$ ceramics with high remnant polarization, J. Alloy. Comp. 610 (2014) 189–195.
[29] W.L. Zhao, R.Z. Zuo, J. Fu, M. Shi, Large strains accompanying field-induced ergodic-polar ordered phase transformations in $Bi(Mg_{0.5}Ti_{0.5})$-$PbTiO_3$-$(Bi_{0.5}Na_{0.5})TiO_3$ ternary system, J. Eur. Ceram. Soc. 34 (2014) 2299–2309.
[30] Y.S. Sung, J.M. Kim, J.H. Cho, T.K. Song, M.H. Kim, T.G. Park, Roles of lattice distortion in $(1-x)(Bi_{0.5}Na_{0.5})TiO_3$-$xBaTiO_3$ ceramics, Appl. Phys. Lett. 96 (2010) 202901.
[31] D. Wang, Y.Z. Wang, Z. Zhang, X.B. Ren, Modeling abnormal strain states in ferroelastic systems: the role of point defects, Phys. Rev. Lett. 105 (2010) 205702.